

Finite element model of fiber volume effect on the mechanical performance of additively manufactured carbon fiber reinforced plastic composites

Adeniran, O, Cong, W, Aremu, D & Oluwole, O

Published PDF deposited in Coventry University's Repository

Original citation:

Adeniran, O, Cong, W, Aremu, D & Oluwole, O 2023, 'Finite element model of fiber volume effect on the mechanical performance of additively manufactured carbon fiber reinforced plastic composites', *Forces in Mechanics*, vol. 10, pp. (In-Press).

<https://doi.org/10.1016/j.finmec.2022.100160>

DOI 10.1016/j.finmec.2022.100160

ISSN 2666-3597

Publisher: Elsevier

This is an Open Access article distributed under the terms of the Creative Commons Attribution License (<http://creativecommons.org/licenses/by/4.0/>), which permits unrestricted use, distribution, and reproduction in any medium, provided the original work is properly cited.



Finite element model of fiber volume effect on the mechanical performance of additively manufactured carbon fiber reinforced plastic composites

Olusanmi Adeniran^{a,*}, Weilong Cong^a, Adedeji Aremu^b, Oluleke Oluwole^c

^a Department of Industrial, Manufacturing and Systems Engineering, Texas Tech University, Lubbock, TX 79409, USA

^b Institute of Advanced Manufacturing and Engineering, Coventry University, UK

^c Department of Mechanical Engineering, University of Ibadan, Nigeria

ARTICLE INFO

Keywords:

Finite element analysis
Computational model
Additive manufacturing
Carbon-fiber-reinforced-plastic-composites
Material properties
Mechanical performance

ABSTRACT

Advancements in additively manufactured (AM) carbon-fiber-reinforced-plastic (CFRP) composites for structural applications require reliable tools to predict mechanical performance. Already, the composites are finding applications in wind turbines, Unmanned Aerial Vehicles (UAVs), space applications, etc., and are promising for more emerging needs. Fiber volume plays a huge role in influencing the mechanical performance of the composites. However, more understanding of their effects are still needed to better ascertain material performance, which can be achieved by applying simulation modeling. This study developed a micromechanical model from Python scripts for Abaqus command line within computer-aided engineering (CAE) environment to predict the composites' structural stability and mechanical performance. The verification of the finite element model by experimental testing showed both the simulation and experimental results to match within an acceptable range. Tensile modulus increased with fiber volume while compressive modulus shows some decreased properties with fiber addition irrespective of fiber content for up to 25% CF volume. The overall results show a possible trade-off between the tensile and compressive properties of the composite, which should be carefully considered in material design for various AM applications.

1. Introduction

1.1. Finite element modeling of CFRP composites fabricated by AM

The reliability of material mechanical properties becomes more important as various developments continue to emerge in the additive manufacturing (AM) of carbon-fiber-reinforced-plastic (CFRP) composites for applications ranging from aerospace to automotive where they are gaining acceptance as alternatives to metallic materials in some structural functions. Finite element analysis (FE) has been applied as a numerical tool for predicting the mechanical performance of engineering materials [1] including CFRP composites and can be applied to the composites fabricated by AM.

The heterogeneity of CFRP composites can greatly increase computational requirements when determining their structural properties via FE, as such it is usually more efficient to approximate the material properties using homogenization techniques. Such techniques require

the selection of a portion of the composite, termed the representative volume element (RVE) in a way that the bulk constitutive properties of the composite are adequately represented in such element and can be used to determine the property of the composite. As illustrated with two RVE choices (RVE A and RVE B) in Fig. 1, the choice of RVE could indeed be diverse, however, the size of RVE is large enough to include intricate features of the material domain. Although evaluation of the RVE properties could be done analytically or empirically, flexibilities inherent in numerical evaluation allow improved control of the modeling process.

As a micromechanical technique, FE requires the imposition of periodic conditions on the boundary of the RVE to reflect the periodicity in the domain. In short-fiber plastic composites, it is common to encounter domains with a rather random distribution of the fiber in the matrix as a consequence of minimal control of fiber location in the manufacturing process. The fibers are mostly randomly distributed, however, from an FE perspective, it is usually sufficient to assume the fibers are periodically distributed in the composite as long as they are evenly spaced in

Abbreviations: AM, Additive Manufacturing; CFRP, Carbon-Fiber-Reinforced-Plastic; CAE, Computer-Aided-Engineering; FE, Finite Element; RVE, Representative Volume Element; CLT, Classical Laminate Theory; ABS, Acrylonitrile-Butadiene-Styrene.

* Corresponding author.

E-mail address: olusanmi.adeniran@ttu.edu (O. Adeniran).

<https://doi.org/10.1016/j.finmec.2022.100160>

Received 18 October 2022; Received in revised form 15 December 2022; Accepted 15 December 2022

Available online 17 December 2022

2666-3597/© 2022 The Author(s). Published by Elsevier Ltd. This is an open access article under the CC BY-NC-ND license (<http://creativecommons.org/licenses/by-nc-nd/4.0/>).

the matrix.

The elastic properties of the RVE are determined by subjecting them to a strain field where opposites faces are subjected to symmetric displacement constraints. The average stress, $\bar{\sigma}$, and strain, $\bar{\epsilon}$ are then determined by averaging them over the RVE as provided by Eqs. (1) and (2). The three-dimensional RVE can be mathematically expressed as:

Eq. (1): Average stress over an RVE

$$\bar{\sigma} = \frac{1}{LBT} \int \sigma_i dv$$

Eq. (2): Average strain over an RVE

$$\bar{\epsilon} = \frac{1}{LB} \int \sigma_i dx$$

where L , B , and T are the length, breadth, and thickness of the RVE, and the effective modulus is determined by dividing Eqs. (1) by (2).

1.2. Current state of development in the simulation modeling of AM fabricated CFRP composites

A sizable number of experimental investigations have reported on the effect of fiber content on the mechanical performance of AM-fabricated CFRP composites [2–8]. However, none has applied a computational method to examine the effect of fiber volume content on the mechanical performance of AM-fabricated CFRP composites. Cuan-Urquizo et al. [9], Turner et al. [10,11], Parandoush et al. [12], and Adeniran et al. [13], conducted detailed reviews of the computational and theoretical modeling approaches to FDM fabricated parts. However, none of the reviewed literature examined fiber volume effects on the mechanical performance of AM-fabricated CFRP composites. Most of the work only considered thermoplastic materials [14–17], with limited work on AM-fabricated CFRP composites.

The two common computational approaches to fiber-reinforced composites found in literature: The microscopic with the microstructure modeled explicitly with as much resemblance to the structure obtained in fabrication [18,19] and the macroscopic where parts are modeled as solid continua with some homogenized effective properties [20] were examined. The fundamental micromechanics computation of the structure allows for the derivation of analytical expressions from which effective Young's modulus and effective shear modulus can be derived for the structure-property relationship.

Other models using theoretical simulations also exist, but the majority of these also examined pure thermoplastics and not CFRP composites. Casavola et al. [21] and Magalhaes [22] used classical laminate theory (CLT) to predict the mechanical performance of partially filled

orthotropic AM fabricated plastics as repeating unit cells and the assumption that the filament rasters are perfectly bonded within a unit cell. Croccolo et al. [23] predicted the mechanical response of 45° raster specimens assuming zero air gap between the rasters. There still remains a knowledge gap in the computational modeling of the mechanical performance of AM-fabricated CFRP composite which this investigation examines. Closing the gaps from the understanding provided in this research will help to improve the development of the manufacturing process for existing and emerging applications and to foster the overall viability of the composites.

1.3. Research motivation

The strength and modulus performance of AM-fabricated CFRP composites are crucial to the development and growth of the composites, making it important to reliably predict their service performance. Hence, the investigation of these mechanical properties. Experimental investigations by the author which examined the effects of fiber content on the mechanical performance of CFRP composites fabricated by AM found increasing fiber content up to 20% to improve the tensile strength and stiffness, but some reduction in compressive strength and modulus. This motivated to explore FE tools to verify the experimental test results.

1.4. Research outline

The paper employed a mixed micromechanical model to investigate the effect of fiber content on the compressive and tensile performance of AM-fabricated CF-ABS composite. It began with a brief description of the general micromechanical modeling of CFRP composites before going on to present a detailed account of the modeling strategy for AM-fabricated CFRP composites using Abaqus and Python.

The results were achieved by automating:

- the generation of a model using representative volume elements (RVE),
- extraction of results from a database, and
- calculations of effective property from results.

The three operations were accomplished via the development of Python scripts for the Abaqus command line in a computer-aided engineering (CAE) environment. The Python scripts eliminated the need for manual model setup while allowing improved control of the modeling process.

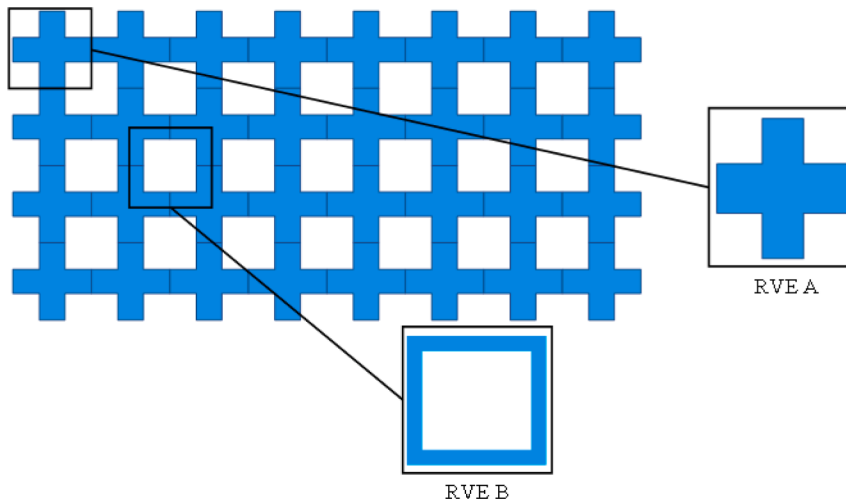


Fig. 1. An illustration of an RVE on a periodic domain.

2. Model development

2.1. Approaches to model development

The investigations could be approached using any of the three different kinds of techniques used in the modeling of fiber-reinforced composites. The microscopic approach models the fibers and matrix separately as deformable continua, however at the expense of extremely high computational cost which makes it uncommon. A second approach applies a macroscopic model with a composite modeled as a single orthotropic material, while a third approach could employ a mixed modeling technique that combines the microscopic and macroscopic modeling of the extruded composite as a stack of series of macroscopically modeled discrete reinforced layers, in which each layer has orthotropic properties.

According to the review of literature on the simulation models of AM-fabricated CFRP composites conducted by Adeniran et al. [13], the mixed-mode approach is more relevant allowing for the interlayer features to be modeled into an RVE. Fig. 2 illustrates the orthotropic stack-up of AM-fabricated CFRP composites (Fig. 3).

Fig. 3 presents the workflow strategy used to achieve the theoretical model results for the fiber volume effect on the mechanical performance of AM-fabricated CFRP composites.

2.2. Micromechanical model generation for AM fabricated CFRP composites

2.2.1. AM process features

Interlayer features are distinguishing factors of the AM fabricated components [7], which influence mechanical performance. The layers are characterized by relatively large triangular voids of similar sizes which are formed as gaps between the print beads during deposition. According to different investigations in the literature [4,24,25], the extent of the porosities is controlled by process factors. Zhang et al. [24] described interlayer porosities to be influenced by raster angles. Ning et al. [4] in their investigation of 0 – 15% CF-ABS composite calculated the porosity value to range from 2 – 10%, while their other study [26] found up to 15% degree of porosity. A preliminary investigation by the author using a micro CT scan found a porosity value range from 11 – 14% for CF-ABS composite fabricated at different deposition temperatures [27]. Thus, an assumption of a 15% degree of porosity for this investigation.

2.2.2. RVE mesh generation

A python script accepting multiple configurations of the fiber

diameter, F_D , fiber length, F_L , fiber volume fraction, V_f , fiber Young's modulus, E_f , matrix Young's modulus, E_m , fiber Poisson ratio, μ_f , matrix Poisson ratio, μ_m , fiber density, D_f , matrix density, D_m was applied to the input values to determine other secondary parameters in the construction of an Abaqus input deck.

A piece of the test specimen as illustrated in Fig. 4 was modeled with an RVE via micromechanical FE, and the RVE was formulated with features sufficient to capture the constitutive characteristics of the overall specimens. The micromechanical FE was achieved by exploiting functionalities within Python and Abaqus software to automate the development of an input deck for a vast number of configurations. Such configuration was applied to explain the effects of the various fiber and matrix material parameters seen in Fig. 3 on the modulus properties of the composite.

The edge length, E_L , of the RVE was determined by Eq. (3) given as:

$$E_L = \alpha F_D$$

Eq. (3): Edge length calculations formula for an RVE where α was a factor used to control the size of the RVE to capture an interlayer. Setting α to 30 was sufficient to assume a dimension of an edge length of an RVE size that fits equal halves of print beads encompassing an interlayer. The number of fibers, N_F , needed to realize a particular V_f was then determined by Eq. (4) given as:

$$N_F = \frac{4V_f E_L^3}{\pi F_D^2 F_L}$$

Eq. (4): Number of fibers calculations for volume fractions

Hexahedral meshing was employed in meshing the domain as shown in Fig. 5 to build an FE model of the resultant mechanical modulus. The model was created from the meshing of domains with prescribed properties and dividing the domain into smaller regions called elements whose properties are more easily determined. The elements were defined by nodes that capture the extent of the elements in the domain, with nodes connecting adjacent elements within the same vicinity and transmitting loads and constraints from one element to another as seen in Fig. 5.

A hexahedral mesh was generated with the edge length, E_L , and the number of elements connected to the edge of the RVE, E_{ax} . Automatically generating a hexahedral mesh allowed the interpretation of the vast number of configurations that could influence the mechanical properties of the composite without incurring large modeling times as observed in manual mesh generation using commercial software. The number of nodes on the edge was therefore set as $E_{ax} + 1$, with the coordinates of the nodes determined between 0 and E_L along the X, Y, and Z cartesian axes. This is illustrated for a $2 \times 2 \times 2$ mesh in Fig. 6a and

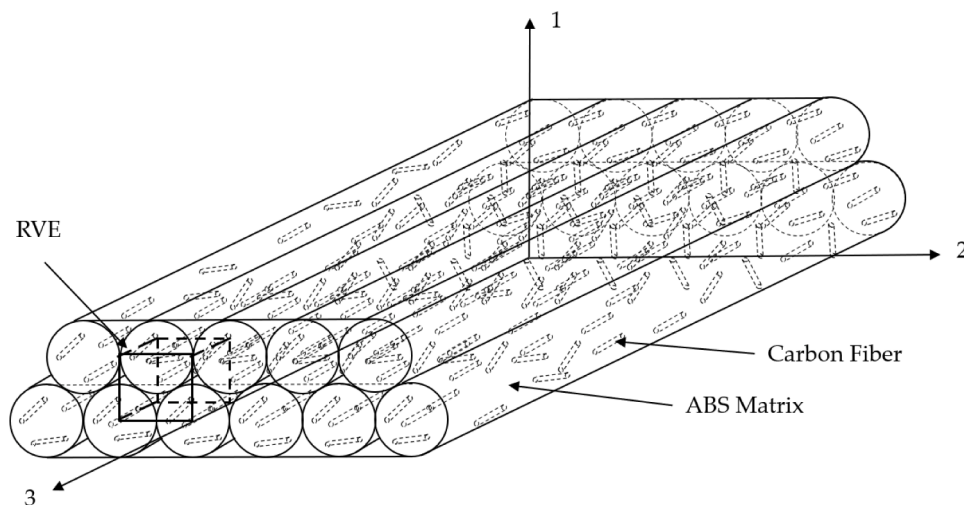


Fig. 2. Orthotropic layer stack-up of AM fabricated CFRP composites [13].

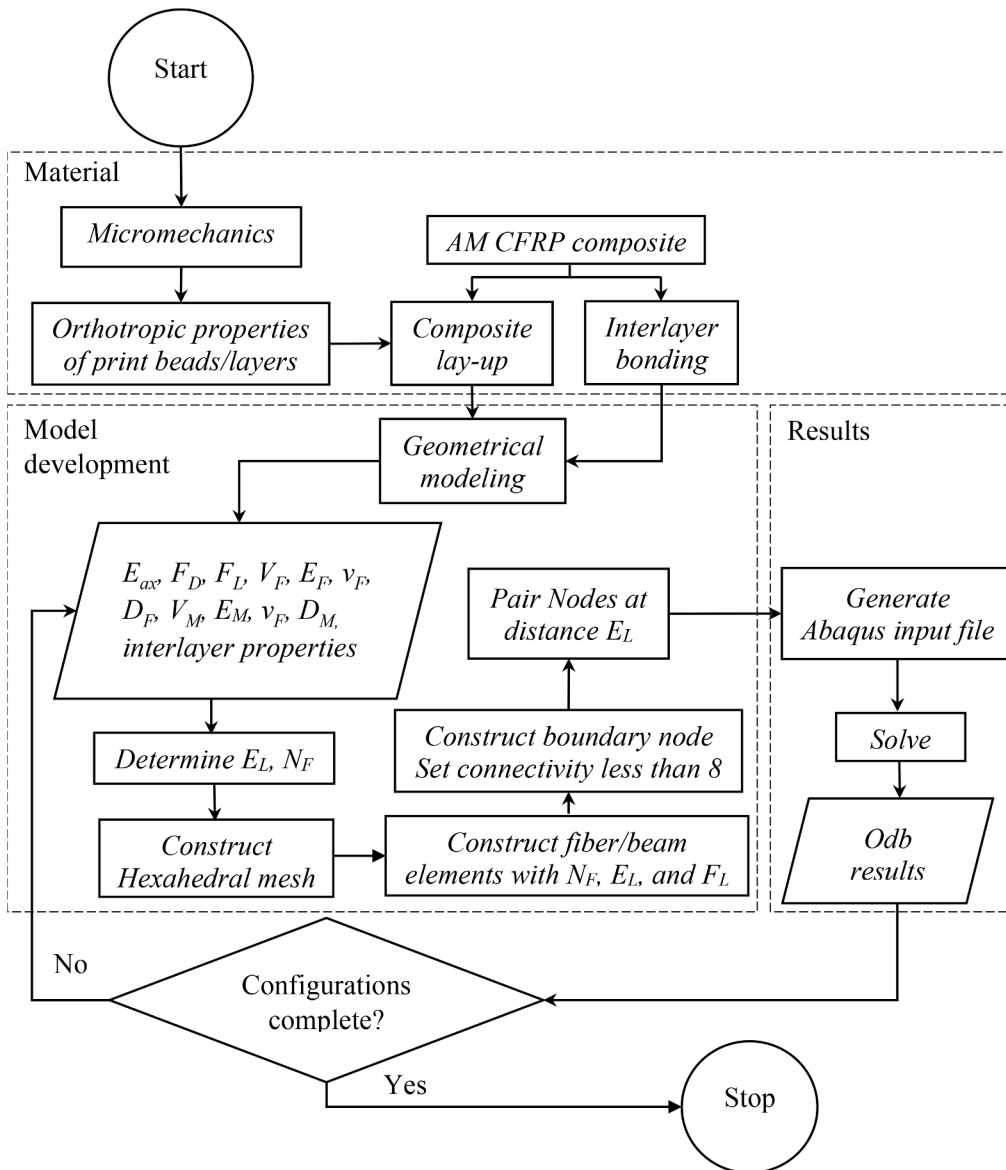


Fig. 3. Flow chart of python script developed to analyze the mechanical properties of the AM fabricated CFRP composite via micromechanical finite element modeling.

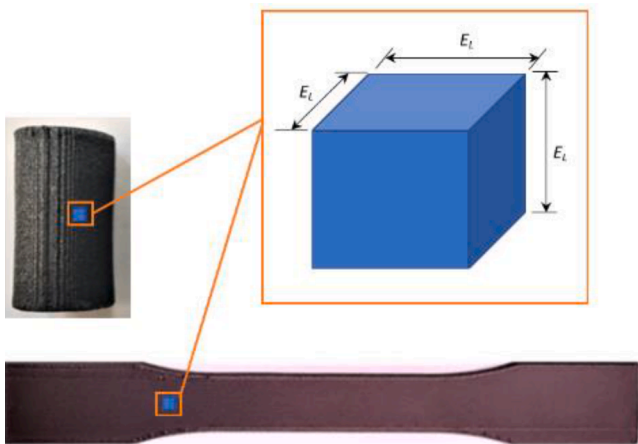


Fig. 4. Features of the Representation Volume Element (RVE) used in the micromechanical FE model.

then combined to realize a regular nodal cloud shown in Fig. 6b.

The nodes were numbered from the bottom up, representing Z equal to 0 planes. Then, from the X and Y equal to E_L planes and then to the X and Y equal to 0 planes. Eight lists of nodes were constructed as the nodes for each hexahedral element with each element having a node in each list. This was achieved by initiating a global list of all nodes and then dissociating boundary nodes that should not belong to a nodal set. The dissociation was achieved by testing nodes at the extrema of the RVE with E_L and then removing them from the nodal sets.

Consequently, the elements array for the $2 \times 2 \times 2$ mesh is:

1	2	4	5	10	11	13	14
2	3	5	6	11	12	14	15
4	5	7	8	13	14	16	17
5	6	8	9	14	15	17	18
10	11	13	14	19	20	22	23
11	12	14	15	20	21	23	24
13	14	16	17	22	23	25	26
14	15	17	18	23	24	26	27

Each row in the matrix shown contains hexahedral elements. The

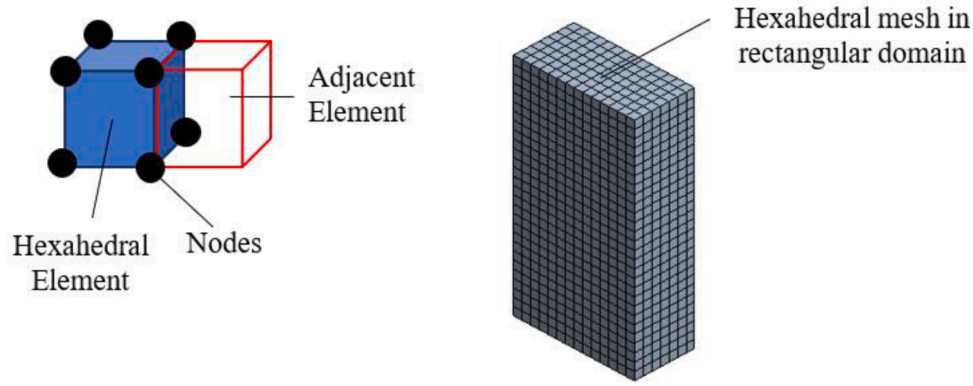


Fig. 5. Illustrations of aspects of the finite element mesh.

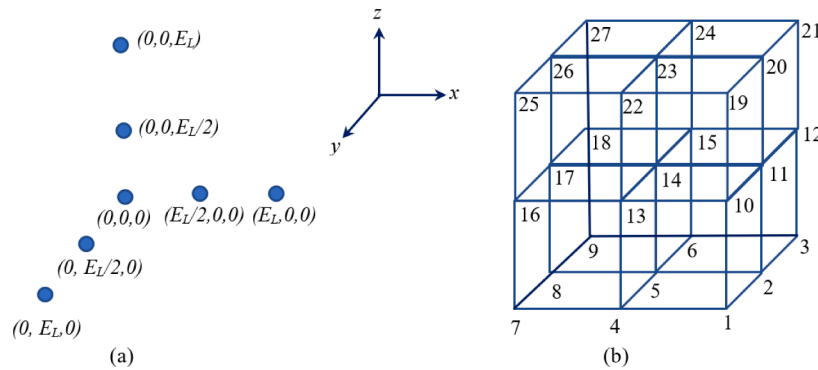


Fig. 6. Illustration of a $2 \times 2 \times 2$ hexahedral mesh generation strategy (a) Axial point vector (b) Emergent hexahedral mesh.

number designates the nodal identification numbers which are the positions of the nodes in another array. A truncated form of the nodes array is:

$$\begin{bmatrix} 0 & 0 & 0 \\ 0 & 0.5E_L & 0 \\ 0 & E_L & 0 \\ \vdots & \vdots & \vdots \\ \vdots & \vdots & \vdots \\ E_L & E_L & E_L \end{bmatrix}$$

The first row is node 1 while the last row is node 27. The meshing strategy offers greater control of the FE by eliminating the need to iteratively generate a new mesh for convergence or parametric studies.

N_F fibers were embedded within the hexahedral mesh by exploiting the Abaqus beam element and embedded element facilities. The fiber locations were randomly generated with respect to the X, Y, and Z cartesian coordinates, with the starting and endpoints lying within the bounds of the RVE, which mathematically can be expressed in Eq. (5) as:

$$0, 0, 0 < X_i, Y_i, Z_i < E_L, E_L, E_L$$

Eq. (5): Fiber location within the X, Y, and Z coordinates. where i is the index of the fiber/ beam.

The endpoint of the fiber/ beam is determined by adding a vector $[0, 0, F_L]$ to its starting point to orient it with respect to the Z-axis. A fiber is accepted into the mesh only if a collision is avoided with other previously generated fibers, as determined by two criteria. The first criterion checks that the X-Y distance (distance calculated from the X and Y coordinates) between the starting point of the fiber is greater than the fiber diameter, F_D , for all existing fibers. The second check ensures the Z distance of the fiber must be greater than F_L and fiber placement in the mesh is only rejected if it fails both acceptance criteria. The fiber element generation stops once the total number of fibers is equal to N_F . A representative configuration of the resulting mesh with fiber hosted

within the bound of a hexahedral is shown in Fig. 7.

The nodes on the beam/ fiber elements are fully embedded within the hexahedral mesh and therefore constrained by the response of these 3D elements. In modeling these fibers, the Abaqus code was applied such that the translational degrees of freedom from the beam elements were removed. As such, the movement at the ends of the beam elements was subject to the translational degrees of freedom of nodes in the hexahedral elements. Load and constraints imposed on the matrix boundaries were therefore correctly transmitted to the beam elements. Hexahedral elements were associated with the properties of the matrix material while the anisotropic properties of carbon fibers were imposed on the beam elements. These properties are presented in Table 1.

Boundary conditions were defined, which involved imposing loads and constraints experienced by the domain at the boundaries. The meshing and imposition of boundary conditions were implemented in a series of equations which were then solved and post-processed. Abaqus software with the capability to minimize the efforts in performing three-dimensional analysis from first principles was employed to realize a satisfactory solution. Young's modulus and Poisson ratio values were applied to construct the elemental stiffness needed to determine the composite's compressive and tensile modulus. Each elemental stiffness was assembled in an array to realize the properties for the entire domain, with the properties of the elements and domains specified in vectors, arrays, and tensors.

Symmetric boundary conditions were imposed on the boundary nodes of the RVE. The boundary nodes were identified by the frequency of the nodal identification numbers in the elements array. Interior nodes were connected to eight elements as illustrated in Fig. 8 while the boundary nodes were connected to less than eight elements in the elements array. The boundary nodes were further classified into surface nodes, edge nodes, and corner nodes which was necessary to impose the appropriate boundary condition on the RVE. The boundary surface

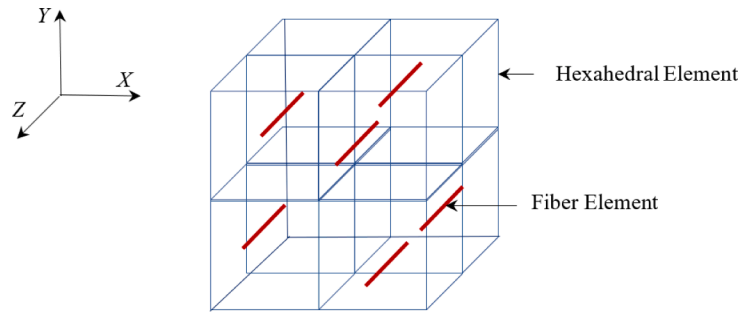


Fig. 7. Emergent mesh: beam/ fiber element hosted with hexahedral elements.

Table 1

Material properties used in the micromechanical FE model (Based on Mattson et al. [28] and Pardini et al. [29]).

Material Property	Axis	Carbon Fiber	ABS
Tensile Modulus (GPa)	X	20.0	3.0
	Y	20.0	3.0
	Z	237.0	3.0
Compressive Modulus (GPa)	X	20.0	10.0
	Y	20.0	10.0
	Z	237.0	10.0
Poisson Ratio	X	0.3	10.0
	Y	0.3	0.3
	Z	0.3	0.3
Fiber Diameter (μm)	-	7	-
Fiber Length (μm)	-	150	-
Density (Ton/mm3)	-	1.33 × 10-9	2.00 × 10-9
Tol (mm)	-	0.05	0.05

nodes were connected to four elements, the boundary edge nodes to two, and the corner nodes were connected to single elements.

Nodes within each class were paired and equation constraints were imposed on the pairs to enforce boundary nodes separated by a distance E_L , displaced by the same amount.

The surface nodes were further classified into six groups namely those on the minimum X, Y, and Z and those on the maximum X, Y, and Z. Fig. 9a illustrates the maximum X, Y, and minimum X, Y planes. Nodes on the maximum planes are paired to another node on its corresponding minimum plane which is at a distance E_L to the node on the maximum plane. The pairing algorithm accepts a set of boundary surface nodes on the maximum plane and the set of surface nodes on its corresponding minimum plane. The distance between the nodes in each set is then calculated using Eq. (6).

$$U_i = \sqrt{(x_{mx} - z_{mn})^2 + (y_{mx} - y_{mn})^2 + (z_{mx} - z_{mn})^2}$$

Eq. (6): Formula for calculating the distance between each nodes set where U_i is the distance of a node in the maximum plane to the i^{th} node in a corresponding minimum plane; mx and mn denote the maximum and minimum planes while x, y, and z represent the coordinate of the nodes in the X, Y, and Z cartesian axes.

The node with $U_i = Z_L$ is paired with the nodes on the maximum plane as shown in Fig. 9. It should be noted that the edge nodes were not included in the first constraining operation and as shown in Fig. 9a were excluded from the colored regions. Also, the maximum and minimum Z planes were also not depicted with colors to enhance the clarity of the image. However, nodes on these planes were paired similarly to those on the X and Y boundary planes as illustrated in Fig. 9b.

In a second operation, nodes on the edge lying on two maximum planes were constrained to the closest node on the diagonally opposite edge which should be the edge lying on the corresponding minimum plane. Fig. 10 depicts paired edges in the modeling operation.

The other edge nodes were also constrained according to Fig. 11, where the edge nodes lying on the intersection of maxima and minima planes were paired and constrained to other edge nodes on a swap of such combinations. For example, the node on Edge K lying on maximum plane X and minimum plane Y was paired and constrained to the closest node on Edge T which exist on minimum plane X and maximum plane Z.

Constraining the edge in this manner minimizes the number of constraint equations required and avoids conflicts between the different constraints. The corners of the RVE cubes were not constrained as a preliminary study suggests this has minimal impact on the simulated results. The distance between paired nodes on all edges was constant for all, with the value determinable from Pythagoras's theorem. This distance is depicted in Fig. 12, showing a projection of the link to the minimum X plane.

Mathematically, the distance between the nodes is given by Eq. (7)

$$U_i = \sqrt{E_L^2 + E_L^2}$$

Eq. (7): Formula for calculating the distance between edge nodes

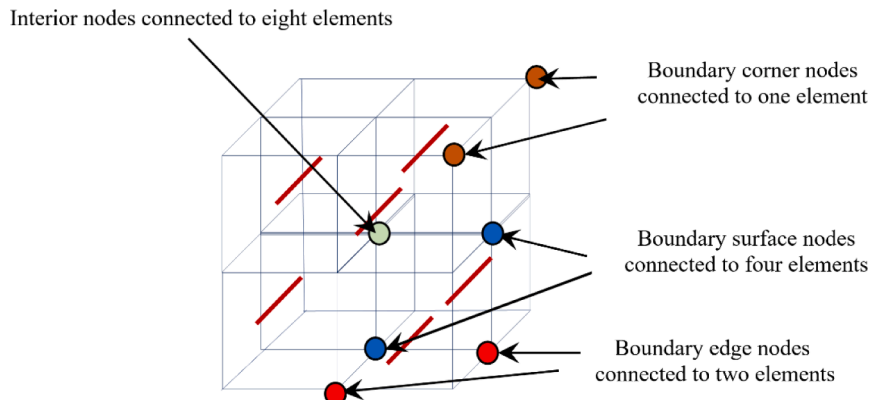


Fig. 8. Classifying boundary nodes based on their element connectivity within an RVE.

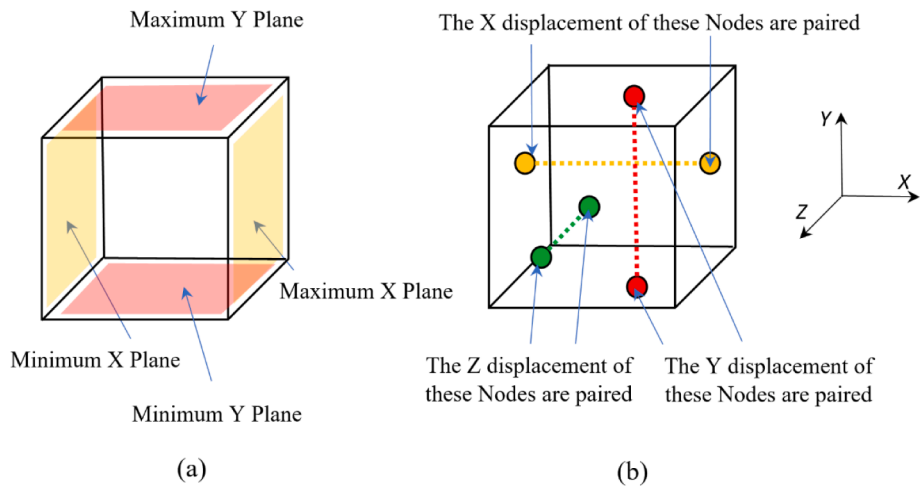


Fig. 9. Illustration of pairing nodes on the maximum and minimum planes of the cartesian coordinate axes.

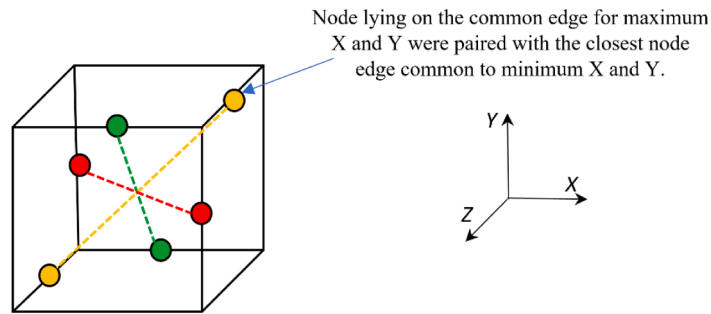


Fig. 10. First operation in constraining edge nodes where edge nodes lying on intersecting maximum planes were paired with their corresponding edge nodes in intersection minimal planes.

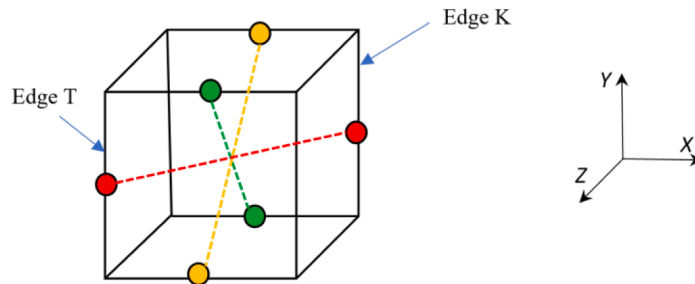


Figure 11. Second operation in constraining edge nodes where edges lying on maximum planes were paired with their corresponding edge in intersection minimal planes.

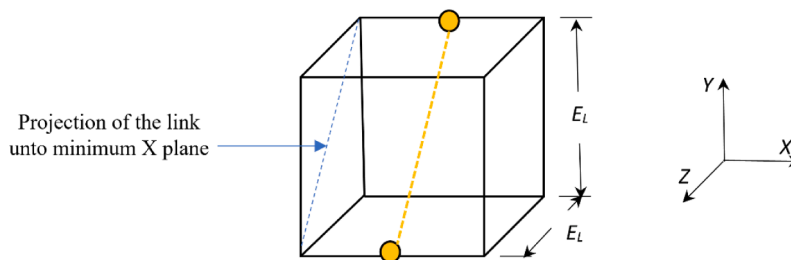


Fig. 12. Illustration of the distance between edge nodes.

A spare node was created at a distance from the RVE which served as the point where a strain is imposed, with the node coordinate set to:

$$[1.2E_L \quad E_L \quad E_L]$$

The 1.2 factor was used to move a node beyond the region occupied by the RVE. This node was constrained to the nodes on the surface of a maximum plane of interest in the iteration with a displacement load imposed on the “spare” node which is transferred to the maximum plane owing to the constraints.

A strain, S_r , -0.0001 was applied at the “spare” node for compression, while a positive strain, S_r , 0.0001 was applied for tension, with the corresponding displacement calculations given by Eq. (8). These displacement calculations were used together with the fiber and matrix material property values presented in Table 1 to simulate both the tensile and compressive modulus results.

$$U = S_r E_L$$

Eq. (8): Displacement calculations for edge nodes

2.3. Experimental investigations

The experimental part of the investigation was conducted by compounding the different percentages of the CF-ABS composites using a Brabender Pre-Center Mixer (CWB Brabender Instruments Inc., Duisburg, Germany). The various fiber composition composite samples were then crushed into smaller bits using a Pelletizer (Fritsch, Idar-Oberstein, Germany) and subsequently extruded into filaments using a filamenting extruder machine (Felfil Evo, Turin, Italy). Details of the experimental test procedure is referenced as part of a different publication by the author [6].

3. Results and discussions

3.1. Results extraction from the database

Simulations using 0.05, 0.10, 0.15, 0.20, and 0.25 carbon fiber volume fractions, V_f , in the ABS matrix were run to better understand the effect of fiber content on the compressive and tensile modulus of the composite. The model data was written to an Abaqus input deck, then solved with the Abaqus command, followed by a mesh convergence study at E_{ax} set as 10, 20, 30, and 40 for all three cartesian axes to

ascertain the effective modulus in the X, Y, and Z directions.

The mesh convergence was done to determine the most suitable mesh for the investigation. The 30^3 edge element was found suitable enough, with the displacement and stress results extracted at this number for the axial modulus calculations. A convergence study was conducted for the X, Y, and Z cartesian axes, respectively in which the material properties were found to be in alignment between the different E_{ax} settings. Fig. 13 shows the results of the convergence study in the Z cartesian axes.

3.2. Discussions of results

The result presents a tensile and compressive modulus evaluation of fiber volume effect on the mechanical performance of AM-fabricated CFRP composites using a finite element model which was further verified with experimental results. The modulus-to-weight ratio of CFRP composites is an important factor in the selection of the composites and the choice of fabrication technique. Hence, the importance of being able to reliably predict this property. The property defines stiffness, which measures the resistance of the material to permanent deformation on the application of force, and at a fundamental level the bond strength between atoms that make up the composite. Such understanding for AM-fabricated CFRP composites is needed to further the knowledge base in the current state of the art of fiber volume effect on the mechanical performance of the composites.

3.2.1. Tensile modulus

The tensile modulus results are presented in Fig. 14. The experimental samples were tested according to ASTM D638 [30], with modulus values measured as a ratio of the applied stress to the resulting strain. Like the compressive modulus, the tensile modulus was calculated from the ratio of initial tensile stress to the corresponding strain, and specifically determined from the slope of the tangent to the elastic region of the curve from the (0,0) origin. The theoretical model was determined by subjecting the RVE to a positive strain field where opposites faces are subjected to symmetric displacement constraints. The average Stress, $\bar{\sigma}$, and strain, $\bar{\epsilon}$ to generate the modulus values determined by averaging across the RVE.

The trends of the results for both the experimental and theoretical model showed an increasing effect of the fiber volume on tensile modulus, which also aligns with reported experimental investigations in

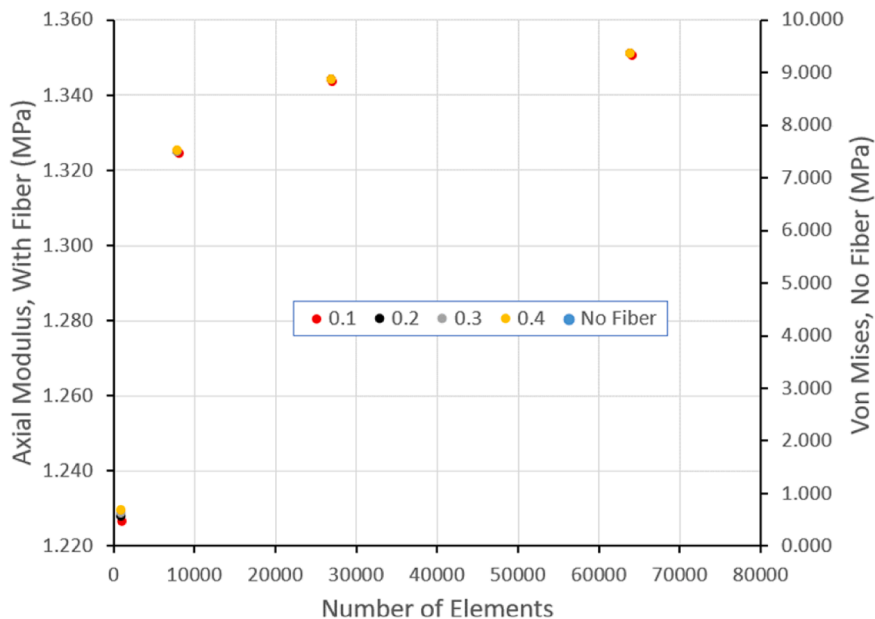


Fig. 13. Mesh convergence study in the Z cartesian axes to ascertain the effective modulus in the orthotropic composite.

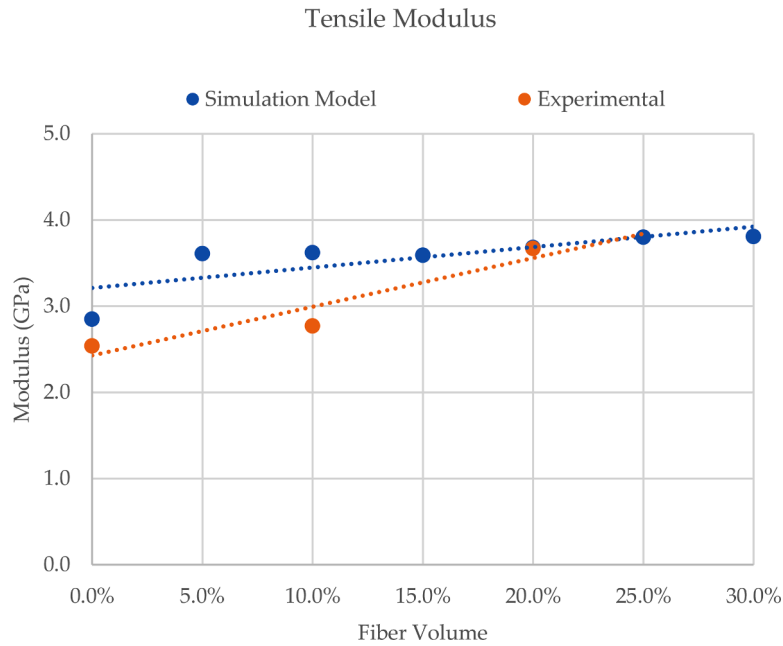


Fig. 14. Experimental investigations versus simulated results comparison for the effect of fiber content on the tensile modulus.

the literature on AM fabricated CFRP composites [2–5,31,32]. However, there were some variances between the experimental and simulated results which could be due to limitations in accurately incorporating some AM process Features such as intra-bead porosities, fiber-matrix interfacial properties, etc., into the simulation model. This inability to accurately measure and incorporate some of the AM process Features into the model accounts for the higher values in the simulated results because in real situations the properties would reduce to be similar to that observed in the experimental result. Data for the experimental investigation was limited to 20% CF due to the ease of fabrication challenges beyond that fiber volume. Also, further development on the model will be required in future tests for more accurate predictions.

The degree of statistical significance for the FE results could not be obtained due to their only being a single FE model. On the other hand, the experimental results seen in Table 2 using the two-sample test ($P \leq 0.005$) show an insignificant effect for 10% fiber volume, but a significant effect thereafter up to 20% CF. The general increase as fiber volume increases can be ascribed to the increasing presence of aligned fibers and their ability to hold the matrix together. Duty et al. [2,31] showed that increasing CF volume to 20% increases the tensile strength and modulus of CF-ABS up to ~66 MPa and ~12 GPa, respectively. Ning et al.'s [4] investigation agrees with this observation for up to 15% of the CF volume that they investigated. Love et al.'s [33] investigation of 13% CF also supports the claim that CF additions increase tensile strength and stiffness, and thermal conductivity, decreased the coefficient of thermal expansion, and greatly reduced the distortion of the parts. Similarly, Mohammadzadeh et al. [32] reported an increase of up to 40% in the tensile strength and 80% modulus properties for AM

fabricated PA matrix reinforced with 8% CF.

3.2.2. Compressive modulus

The result for the compressive modulus is presented in Fig. 15. The experimental results were measured from the ratio of the applied stress to the resulting strain in samples tested according to ASTM D695 [34]. The modulus values for the different fiber contents were calculated from the ratio of initial stress to the corresponding strain, specifically determined from the slope of the tangent to the elastic region of the curve from the (0,0) origin.

For the FE model, the compressive modulus was determined by subjecting the RVE to a strain field where opposite faces are subjected to symmetric displacement constraints. The average Stress, $\bar{\sigma}$, and strain, $\bar{\epsilon}$ to generate the modulus values were then determined by averaging over the RVE.

While the experimental results show some decrease in compressive modulus with the fiber additions irrespective of fiber volume for the 10% CF – 30% CF tested, results from the theoretical model also show a reducing but insignificant effect of fiber addition. The differences in the experimental and theoretical results could be accounted for by recognizing that there is insufficient information to accurately measure and include certain AM features such as intra-bead porosities, fiber-matrix interfacial strength, etc. in the current FE model.

Just as was seen with the tensile results, the degree of significance testing for compressive modulus could not be obtained for the FE results due to only one data point generation feature of the model. However, a visual examination of the FE model data trends suggests an insignificant effect for fiber additions up to 30% CF. The experimental results on the other hand using a two-sample test as seen in Table 3 show a negative significant effect of fiber additions irrespective of the fiber volume for the 10 – 30 % CF investigated. This negative effect in compression which is different from that seen in tension is from the difference in the effective fiber function and fiber-matrix interface deformation under the two different loading modes. Hence, the difference in effective fiber actions under the different loading modes.

The reduction in the experimental compressive modulus with fiber additions corresponds to a similar result from studies by Mohammadi-zadeh et al. [32] which compared the compressive properties of AM fabricated PA with those containing 15% CF volumes of short fiber and also continuous fiber. They found a reduction in the compressive

Table 2 Degree of significance testing of tensile modulus from fiber volume effect.

Modulus (GPa)	Axial Tensile			
Fiber Volume	ABS (0%)	10%	20%	30%
Mean	2.54	2.77	3.70	-
Variance	0.05	0.02	0.01	-
Observations	5	5	5	-
Df	3	4	-	-
t Stat	-1.524	-8.952	-	-
P(T≤t) two-tail		0.225	0.001	-
t Critical two-tail		3.182	2.776	-

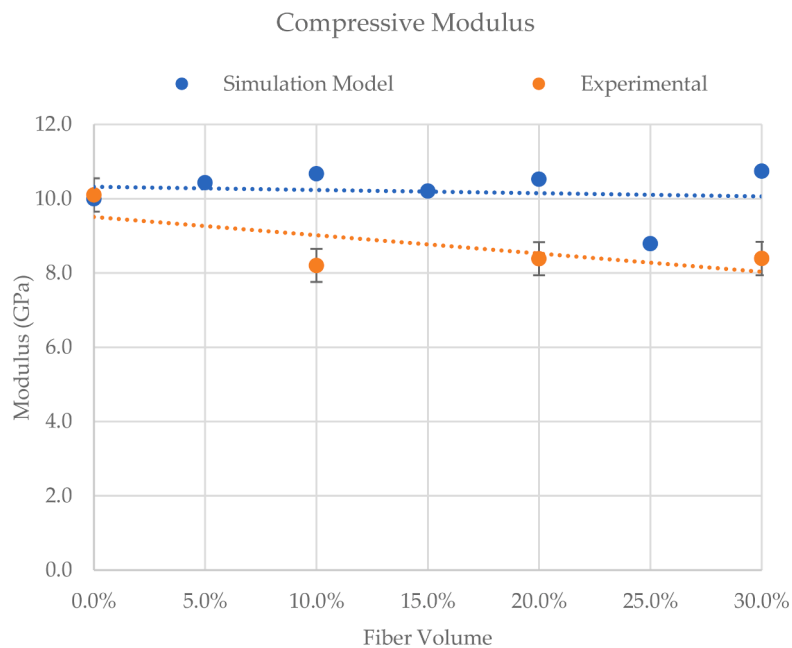


Fig. 15. Experimental investigations versus simulated results comparison for the effect of fiber content on the compressive modulus of AM-fabricated CFRP composites.

Table 3 Degree of significance testing of compressive modulus from fiber volume effect.

Modulus (GPa) Fiber Volume	Axial Compression			
	ABS (0%)	10%	20%	30%
Mean	10.1	8.2	8.4	8.4
Variance	0.9	0.0	0.2	0.3
Observations	5	5	5	5
Df		3	4	6
t Stat		4.123	-0.836	-0.013
P(T≤t) two-tail		0.026	0.450	0.990
t Critical two-tail		3.182	2.776	2.447

modulus of both short and continuous fiber CF-PA composites, which they ascribed to micro-buckling, matrix-fiber splitting, and fiber kinking as the main cause of failures in the compression of AM-fabricated CFRP composites. They related stress concentration at the fiber ends due to the application of compressive load as the main cause of premature failure, where the stress concentrations result in the generation of cracks at the interface of fiber and matrix to weaken the part. Studies by Thompson, Fletch et al. [35–37] for compression molded parts also found the roles of small imperfections, such as porosity and fiber misalignment in the formation of kink bands which are present in CFRP composites to affect compressive modulus. However, the absence of micro buckling and fiber kinking in the tensile mode resulted in higher tensile strength with fiber additions. The kink bands are absent in tension but in compression where they serve as stress concentration points to reduce material properties.

The existence of the weaker fiber-matrix interlayer regions in CFRP composites creates reduced mechanical strength in the compression mode which is subjected to shearing actions. This is against the activity in pure matrix material where the weak fiber-matrix interlayer region is absent, and bonding is between the material of the same surface energies and interlayer compatibilities. The theory of fiber-matrix interfacial effects on compressively loaded composites proposed by Greszczuk [38] can be applied to explain the reducing compressive strength with increasing fiber content in AM fabricated CFRP composites. This is because compression loading more easily affects the fiber-matrix interface because of the shearing nature of failure propagation typical of the loading mode. They presented both experimental and theoretical studies

on the failure modes of compressively loaded composites to support the theory that the composites exhibit much lower strength than predicted by the micro buckling theory. This is the result of the lower fiber-matrix interface properties which are much lower than the average properties of the entire composite.

4. Conclusions

In this study, the micromechanical model which considered Python scripts for the Abaqus command line in a computer-aided engineering (CAE) environment was used to confirm experimental results which investigated the compressive and tensile modulus of AM fabricated CFRP composite. The conclusions drawn are as follows:

- 1 Tensile modulus increases in an upward trend with fiber additions as determined from the experimental and theoretical investigations for the up to 20% fiber volume examined.
- 2 Compressive modulus is insignificantly or negatively imparted by fiber additions from the FE observation of insignificant fiber addition effects and the experimental observation of a reduction in modulus with increasing fiber volume.
- 3 The differences in the tensile and compressive modulus trends can be ascribed to the differences in the effective fiber characteristics under the two different loading modes.
- 4 In considering AM fabricated CFRP composites, there are some trade-offs between tensile and compressive properties, which should be given due consideration in materials design.

Funding

This research received no specific grant from any funding agency in the public, commercial, or not-for-profit sectors.

Declaration of Competing Interest

The authors declare that they have no known competing financial interests or personal relationships that could have appeared to influence the work reported in this paper.

Data availability

Data will be made available on request.

References

- [1] S. Moaveni, *Finite Element analysis: Theory and Application*, 4th ed., Pearson, Upper Saddle River, NJ, 2015.
- [2] C.E. Duty, V. Kunc, B. Compton, B. Post, D. Erdman, R. Smith, et al., Structure and mechanical behavior of big area additive manufacturing (BAAM) materials, *Rapid. Prototyp. J.* 23 (2017) 181–189, <https://doi.org/10.1108/RPJ-12-2015-0183>.
- [3] N. van de Werken, H. Tekinalp, P. Khanbolouki, S. Ozcan, A. Williams, M. Tehrani, Additively manufactured carbon fiber-reinforced composites: State of the art and perspective, *Addit. Manuf.* 31 (2020), <https://doi.org/10.1016/j.addma.2019.100962>.
- [4] F. Ning, W. Cong, J. Qiu, J. Wei, S. Wang, Additive manufacturing of carbon fiber reinforced thermoplastic composites using fused deposition modeling, *Compos. B Eng.* 80 (2015), <https://doi.org/10.1016/j.compositesb.2015.06.013>.
- [5] A.A. Hassen, J. Lindahl, X. Chen, B. Post, L. Love, V. Kunc, Additive manufacturing of composite tooling using high temperature thermoplastic materials, *Int. SAMPE Tech. Conf.* (2016), 2016-Janua.
- [6] O. Adeniran, W. Cong, E. Bediako, V. Aladesanmi, Additive manufacturing of carbon fiber reinforced plastic composites: the effect of fiber content on compressive properties, *J. Compos. Sci.* 5 (2021) 325, <https://doi.org/10.3390/jcs5120325>.
- [7] O. Adeniran, W. Cong, K. Oluwabunmi, Thermoplastic matrix material influences on the mechanical performance of additively manufactured carbon fiber reinforced plastic composites, *J. Compos. Mater.* 56 (2022), <https://doi.org/10.1177/002199832211077345>.
- [8] Adeniran O. Mechanical Performance of Carbon Fiber Reinforced Plastic Composites Fabricated by Additive Manufacturing. Texas Tech University, 2022. <hdl.handle.net/2346/90141>.
- [9] E. Cuan-Urquizo, E. Barocio, V. Tejada-Ortgoza, R.B. Pipes, C.A. Rodriguez, A. Roman-Flores, Characterization of the mechanical properties of FFF structures and materials: a review on the experimental, computational and theoretical approaches, *Materials* 12 (2019), <https://doi.org/10.3390/ma12060895>.
- [10] B.N. Turner, S.A. Gold, A review of melt extrusion additive manufacturing processes: II. Materials, dimensional accuracy, and surface roughness, *Rapid Prototyp. J.* 21 (2015), <https://doi.org/10.1108/RPJ-02-2013-0017>.
- [11] B.N. Turner, R. Strong, S.A. Gold, A review of melt extrusion additive manufacturing processes: I. process design and modeling, *Rapid Prototyp. J.* 20 (2014) 192–204, <https://doi.org/10.1108/RPJ-01-2013-0012>.
- [12] P. Parandoush, D. Lin, A review on additive manufacturing of polymer-fiber composites, *Compos. Struct.* 182 (2017) 36–53, <https://doi.org/10.1016/j.compstruct.2017.08.088>.
- [13] O. Adeniran, W. Cong, A. Aremu, Material design factors in the additive manufacturing of short carbon fiber reinforced plastic composites: a state-of-the-art-review, *Adv. Ind. Manuf. Eng.* 5 (2022), 100100, <https://doi.org/10.1016/j.aime.2022.100100>.
- [14] Zhang Y., Chou Y. Three-dimensional finite element analysis simulations of the fused deposition modelling process: 2006;220:1663–71. [10.1243/09544054JEM572](https://doi.org/10.1243/09544054JEM572).
- [15] A.H. Nickel, D.M. Barnett, F.B. Prinz, Thermal stresses and deposition patterns in layered manufacturing, *Mater. Sci. Eng. A* 317 (2001) 59–64, [https://doi.org/10.1016/S0921-5093\(01\)01179-0](https://doi.org/10.1016/S0921-5093(01)01179-0).
- [16] Zhang Y., Chou K. A parametric study of part distortions in fused deposition modelling using three-dimensional finite element analysis: 2008;222:959–67. [10.1243/09544054JEM990](https://doi.org/10.1243/09544054JEM990).
- [17] Huang B., Singamneni S. Adaptive slicing and speed- and time-dependent consolidation mechanisms in fused deposition modeling: 2013;228:111–26. [10.1177/0954405413497474](https://doi.org/10.1177/0954405413497474).
- [18] C. Wendt, A.P. Valerga, O. Droste, M. Batista, M. Marcos, FEM based evaluation of fused layer modelling monolayers in tensile testing, *Procedia Manuf.* 13 (2017) 916–923, <https://doi.org/10.1016/J.PROMFG.2017.09.160>.
- [19] M. Somireddy, A. Czekanski, Mechanical characterization of additively manufactured parts by FE modeling of mesostructure, *J. Manuf. Mater. Process.* 1 (2017) 18, <https://doi.org/10.3390/JMMP1020018>. Page2017;1:18.
- [20] M. Domingo-Espin, J.M. Puigoriol-Forcada, A.A. Garcia-Granada, J. Llumà, S. Borros, G. Reyes, Mechanical property characterization and simulation of fused deposition modeling polycarbonate parts, *Mater. Des.* 83 (2015) 670–677, <https://doi.org/10.1016/J.MATDES.2015.06.074>.
- [21] C. Casavola, A. Cazzato, V. Moramarco, C. Pappalettere, Orthotropic mechanical properties of fused deposition modelling parts described by classical laminate theory, *Mater. Des.* 90 (2016) 453–458, <https://doi.org/10.1016/J.MATDES.2015.11.009>.
- [22] L.C. Magalhães, Evaluation of stiffness and strength in fused deposition sandwich specimens, *J. Br. Soc. Mech. Sci. Eng.* 36 (2013) 449–459.
- [23] D. Crococolo, M. de Agostinis, G. Olmi, Experimental characterization and analytical modelling of the mechanical behaviour of fused deposition processed parts made of ABS-M30, *Comput. Mater. Sci.* 79 (2013) 506–518, <https://doi.org/10.1016/J.COMMATSCI.2013.06.041>.
- [24] W. Zhang, C. Cotton, J. Sun, D. Heider, B. Gu, B. Sun, et al., Interfacial bonding strength of short carbon fiber/acrylonitrile-butadiene-styrene composites fabricated by fused deposition modeling, *Compos B Eng* 137 (2018) 51–59, <https://doi.org/10.1016/j.compositesb.2017.11.018>.
- [25] H.L. Tekinalp, V. Kunc, G.M. Velez-Garcia, C.E. Duty, L.J. Love, A.K. Naskar, et al., Highly oriented carbon fiber-polymer composites via additive manufacturing, *Compos Sci. Technol.* 105 (2014) 144–150, <https://doi.org/10.1016/j.compscitech.2014.10.009>.
- [26] F. Ning, W. Cong, Z. Hu, K. Huang, Additive manufacturing of thermoplastic matrix composites using fused deposition modeling: a comparison of two reinforcements, *J. Compos. Mater.* 51 (2017) 3733–3742, <https://doi.org/10.1177/0021998317692659>.
- [27] O. Adeniran, N. Osa-uwagboe, W. Cong, M. Ramoni, Fabrication temperature-related porosity effects on the mechanical properties of additively manufactured CFRP composites, *J. Compos. Mater.* 7 (2023) 1–17.
- [28] D. Mattsson, R. Joffe, J. Varna, Damage in NCF composites under tension- effect of layer stacking sequence, *Eng. Fract. Mech.* 75 (2008) 2666–2682, <https://doi.org/10.1016/j.engfracmech.2007.03.014>.
- [29] L.C. Pardini, M.L. Gregori, Modeling elastic and thermal properties of 2.5D carbon fiber and carbon/SiC hybrid matrix composites by homogenization method, *J. Aeronaut. Technol. Manag.* 2 (2010) 183–194, <https://doi.org/10.5028/jatm.2010.02026510>.
- [30] ASTM INTERNATIONAL. ASTM D638-14. Annual Book of ASTM Standards 2014: 1–17. [10.1520/D0638-14.1](https://doi.org/10.1520/D0638-14.1).
- [31] C.E. Duty, F. Tom, A. Franc, Material Development for Tooling Applications Using Big Area Additive Manufacturing (BAAM), OAK Ridge National Laboratory, 2015, pp. 1–8, <https://doi.org/10.2172/1209207>.
- [32] M. Mohammadzadeh, A. Gupta, I. Fidan, Mechanical benchmarking of additively manufactured continuous and short carbon fiber reinforced nylon, *J. Compos. Mater.* 55 (2021) 3629–3638, <https://doi.org/10.1177/00219983211020070>.
- [33] L.J. Love, V. Kunc, O. Rios, C.E. Duty, A.M. Elliott, B.K. Post, et al., The importance of carbon fiber to polymer additive manufacturing, *J. Mater. Res.* 29 (2014) 1893–1898, <https://doi.org/10.1557/jmr.2014.212>.
- [34] ASTM International, Compressive properties of rigid plastics, *Ann. Book ASTM Stand.* (2008) 1–8, <https://doi.org/10.1520/D0695-15.2>, i.
- [35] N. Fleck, L. Deng, B. Budiansky, Prediction of kink width in compressed fiber composites, *J. Appl. Mech.* 62 (1995) 329–337, <https://doi.org/10.1115/1.2895935>.
- [36] K.H. Lo, E.S.M. Chim, Compressive strength of unidirectional composites, *J. Reinf. Plast. Comp.* 11 (1992) 838–896, <https://doi.org/10.1177/073168449201100801>.
- [37] Thompson R. Compressive Strength of Continuous Fiber Unidirectional Composites. Ph.D. Thesis. Clemson University, 2012. tigerprints.clemson.edu/all_dissertations/953.
- [38] Greszczuk L.B. On failure modes of unidirectional composites under compressive loading. *Fract. Comp. Mater.*, 1982, p. 231–44. [10.1007/978-94-009-7609-2_19](https://doi.org/10.1007/978-94-009-7609-2_19).